J. Fluid Mech. (1992), *vol.* 235, *pp.* 399–414
Printed in Great Britain

Droplet spreading on a thin viscous film

By DONALD P. GAVER III[1] AND JAMES B. GROTBERG[2]

[1] Department of Biomedical Engineering, Tulane University, New Orleans, LA 70118, USA

[2] Biomedical Engineering Department, Northwestern University, Evanston, IL 60208, USA and Department of Anesthesia, Northwestern University Medical School, Chicago, IL 60611, USA

(Received 17 September 1990 and in revised form 19 April 1991)

We investigated experimentally the flows induced by a localized surfactant (oleic acid) on thin glycerol films. The oleic acid creates surface-tension gradients, which drive convention on the surface and within the film. Qualitative descriptions of the Lagrangian flow field were provided by flow-visualization experiments. Quantitative measurements of surface flows were conducted using dyed glycerol markers, where the initial motion of these markers is used to define the position of the time-dependent 'convection front'. The flow characteristics were found to depend largely upon the magnitude of a gravitational parameter, G, representing the ratio of gravitational to surface-tension gradient (Marangoni) forces. Small G ($G < 0.5$) caused net outflow of the film leading to this thinning and, in some cases, to film rupture. When $G < 1$, bi-directional flows were caused by hydrostatic pressure gradients which served to stabilize the film. Additionally, the position of a surface convection front was found to differ significantly from that of the surfactant's leading edge for all $G > 0$. For this reason, surface markers may not be used to measure accurately the position of the droplet's leading edge. Finally, simulations of the Lagrangian flows conducted using the theory of Gaver & Grotberg (1990) compare favourably with these experimental results in the limit of dilute surfactant concentrations, and thus experimental verification of that theory is provided by this work. The results of this study may be useful for understanding the behaviour of the lung's thin-film lining after an aerosol droplet of insoluble exogenous surfactant lands upon its surface.

1. Introduction

Medication mists are commonly used safely and effectively for the delivery of pharmaceutical agents. Once inhaled, the aerosol droplets that comprise this mist travel down the bronchial tree, and eventually deposit on the bronchial walls and alveoli, through which they deliver their contents to the airway wall and bloodstream. This delivery technique is particularly well suited for treatment of pulmonary diseases and their symptoms. For instance, bronchodilating chemicals are frequently delivered in this manner for the treatment of asthma. Recently, aerosol inhalation has been used to deliver antibiotics to patients with Acquired Immune Deficiency Syndrome (AIDS) (Conte, Hollander & Golden 1987). Additionally, delivery of aerosolized surfactants may help treat premature neonates suffering from hyaline membrane disease, which is caused by an abnormally high surface tension of the lung's liquid lining owing to the immature lung's inability to produce adequate quantities of surfactant. Finally, the delivery of surfactant may be useful in reopening the pulmonary airways of both neonates and patients suffering

from airway obstructive diseases, since lowering the surface tension of the airway lining fluid will decrease the capillary forces that hold opposing airway walls together. Thus the delivery of surfactant to closed airways may allow those airways to be more easily reopened, increasing their capacity to contribute to gas exchange (Gaver, Samsel & Solway 1990). Surfactant replacement therapy has been shown to decrease dramatically the mortality of respiratory distress syndrome (Avery & Merritt 1991).

Previous analysis of the droplet/thin-film system have modelled the droplet as a localized surfactant that decreases the local interfacial surface tension of a thin viscous film. Surfactant concentration gradients create surface-tension gradients that induce Marangoni convection which spreads the droplet along, and drives flows within, the thin film. Borgas & Grotberg (1988) presented a theory of steady-state spreading of an insoluble droplet and used these results to make predictions of the time-dependent spreading rate. Subsequently, Gaver & Grotberg (1990) investigated the time-dependent flows of insoluble droplets, and presented information concerning the Eulerian flow field. Both studies showed that surfactant-induced flows modify the film's thickness, and suggested the possibility that droplet contaminant (medication or toxin) transport may be modified by the flows within the thin film. Halpern & Grotberg (1990) have recently extended this work to include the effects of surfactant solubility.

Experimental investigations of droplet spreading on thin films have been published by Ruckenstein, Smigelschi & Suciu (1970), Ahmad & Hansen (1972), Hussain, Fatima & Ahmad (1975) and Fraaije & Cazabat (1989). All of these studies commence with large volumes of surfactant (surface concentrations much greater than the saturation monolayer concentration) and do not provide detailed information concerning the surface-activity of the droplet. It is thus not possible to compare the results of these experimental studies to theoretical calculations that rely upon the description of droplet initial conditions and surface activity. Additionally, these studies do not report information concerning the convection field within the film substrate.

In this paper we present our experimental investigation of the time-dependent flows induced by a localized surfactant on a thin film. Qualitative observations are used to characterize the thin-film flow field for different values of film thickness, and quantitative studies examine the surface flows. In § 2 the flow-visualization and quantitative surface-flow measurement experiments are described, and the data from these experiments are presented in § 3. In §4 the theory of Gaver & Grotberg (1990) is briefly outlined and predictions from that theory are compared with the experimental results. Finally, the conclusions are presented in § 5, where the findings of this study are related to the delivery of medication by aerosol inhalation.

2. Methods

2.1. *Flow visualization*

We studied the qualitative behaviour of oleic acid droplets spreading on thin glycerol films by flow visualization. A glycerol layer of thickness H_0 (1 or 2 mm) was established in a 13.8 cm diameter glass Petri dish. In order to visualize the surface flow, the glycerol film was dusted with talc and to visualize the flow near the bottom, parallel dye streaks (Luma permanent scarlet water colour) were injected along the bottom of the Petri dish using a micropipette. All experiments commenced with the deposition of 1 drop (≈ 30 μl) of oleic acid. As the oleic acid (surfactant) spread, the

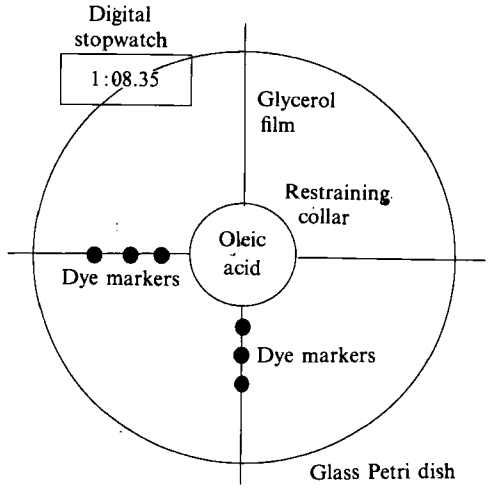

FIGURE 1. Schematic of the flow measurement apparatus.

Set	R_0 (mm)	H_0 (mm)	V_{surf} (10^{-4} µl)
A	16.0	2.0	18.4
B	7.5	0.7	9.2

TABLE 1. Initial conditions of experiments A and B

talc remained on the surface, and convected with the surface. Concurrently, the dye streaks deformed as they were transported by the flow within the film, thus indicating the flow direction near the wall. In a third experiment, the film layer was set at $H_0 = 0.4$ mm, and the glycerol was dyed uniformly rather than with streaks (the creation of which were mechanically disruptive to the extremely thin film). This flow-visualization method allowed the qualitative film thickness to be interpreted by the transmittance of light through the film.

2.2. *Flow measurement*

Quantitative measurements of surface flows were conducted using the apparatus shown schematically in Figure 1. Films of two thicknesses, $H_0 = 2.0$ mm and 0.7 mm, were studied, and are hereinafter referred to as experiments A and B, respectively. A removable restraining collar of radius R_0 was placed in the centre of the Petri dish, physically isolating the film on the inside of the collar from that on the outside. Oleic acid was deposited on the interface confined by this collar, which thus set the initial radius of the localized surfactant. The restraining collar permitted delivery of the oleic acid in a dilute solution of hexane, which was allowed to evaporate before the experiment commenced. This methodology allowed the study of monolayers whose concentrations were small, and allowed the initial droplet radius to be set much larger than the initial film thickness ($R_0 \gg H_0$). The initial conditions for these experiments are summarized below in table 1, where V_{surf} is the volume of the surfactant. These initial conditions correspond with those posed theoretically by Gaver & Grotberg (1990), and thus permit the comparison of the experimental results with predictions from that theory. Surface flows were visualized by dyed-glycerol

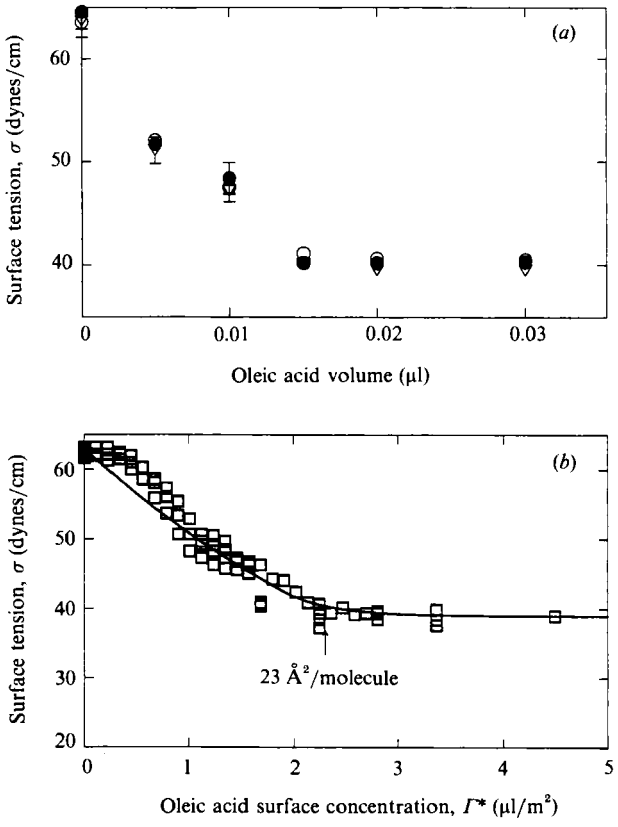

FIGURE 2. Surface activity of oleic acid on glycerol. (*a*) Investigation of solubility. Air–liquid interfacial area = 71 cm². ○, Glycerol volume = 20 ml; ●, 40 ml; ▽, 60 ml. (*b*) Relationship between surface concentration and interfacial surface tension for oleic acid on glycerol; —— represents equation (4.5).

markers (Luma permanent scarlet water colour), placed on the film surface at radial distances of $r_A = 2.5$, 3.0, 3.5 and 4.0 cm and $r_B = 1.5$, 2.0 and 2.5 cm, where the subscripted A or B denotes the experimental set. The dye markers were selected to be non-surface-active, and caused no noticeable convection in the film layer upon their deposition. These dye markers were used instead of the more commonly used talc, because it was found that talc retarded the surface flows and thus influenced the rates of droplet spreading. Experiments commenced by manually lifting the restraining collar, allowing the surfactant to spread. The experiments were recorded with a Panasonic WV-555 video camera and Sony Model VO-5800 $\frac{3}{4}$-inch video recorder. Slow motion playback of the experiments allowed accurate measurement of the onset of motion of each of the flow-visualization markers. Thus, the data consist of the time of the initial surfactant release and the times at which each of the flow-visualization markers first moved. These data provide a measure of the onset time for convection (to be defined below) at fixed radial positions from the centre of the surfactant source.

2.3. *Measurement of surface tension vs. surfactant concentration*

The flows investigated in this study are driven by surface-tension gradients, whose magnitude depends upon the concentration gradients of the surfactant (oleic acid) in concert with the surface-tension equation of state, the relationship between surface

tension and surfactant concentration. This relationship was measured using a Wilhelmy balance after deposition of small quantities of oleic acid on the surface of a glycerol film. Because of its large surface activity, the pure oleic acid was first diluted in hexane to ratios of $1:10^4$ and $1:10^5$ (oleic acid:hexane) before depositing small aliquots of these solutions (5–20 μl) onto the film contained within a glass Petri dish. The surface tension was measured 4–5 min after deposition to allow the hexane to evaporate and the surface tension to reach equilibrium. To evaluate the solubility of oleic acid in glycerol, small volumes of oleic acid were deposited onto glycerol films possessing identical air–liquid interfacial areas (71 cm^2), but different film volumes. Figure 2(*a*) shows that the measured surface tension was insensitive to the film volume, indicating that oleic acid formed an insoluble monolayer upon glycerol. Thus, the initial surface-concentration was simply $\Gamma_0^* = V_{surf}/A$, where V_{surf} is the volume of oleic acid, A is the surface area of the glycerol film, and * denotes a dimensional quantity. The empirically determined surface-tension equation of state is shown in figure 2(*b*). The surface tension of the 'clean' glycerol surface is $\sigma_0 \approx 63$ dynes/cm. As the surfactant concentration (Γ^*) increases, the surface tension (σ^*) decreases monotonically until $\Gamma^* = \Gamma_m = 2.3$ μl/m^2. For $\Gamma^* > \Gamma_m$, the surface tension is relatively constant, with a magnitude of $\sigma^*(\Gamma_m) = \sigma_m = 39$ dynes/cm, implying that the oleic acid molecules are in a close-packed, or 'micelle' formation at $\Gamma^* = \Gamma_m$. This concentration provides an intermolecular spacing of 23Å^2/molecule, a value in agreement with Gaines (1966) and Agrawal & Neuman (1988). For large drops of surfactant, the constancy of σ^* for $\Gamma^* > \Gamma_m$ removes the Marangoni forcing within the central region of a 'macroscopic' drop, and thus explains why the precursor monolayer film determines the droplet spreading rate (Fraaije & Cazabat 1989).

Since hexane was used as a delivery medium for the oleic acid, the surface tension of glycerol contaminated with hexane (1 ml pure hexane) was measured. While hexane initially lowered the surface tension, after evaporation (≈ 1 min) the surface tension returned to that of the clean glycerol film. Precautions were thus made to avoid flow measurements during the evaporation phase.

3. Results

3.1. *Qualitative flow patterns*

Figures 3(*a*) and 3(*b*) illustrate the Lagrangian flow patterns that arise approximately 30 s subsequent to the deposition of pure oleic acid, after which motion had nearly ceased. Recall that the dye streaks were placed near the bottom wall, and talc was sprinkled on the glycerol surface. Figure 3(*a*) ($H_0 = 2$ mm) demonstrates bidirectional flow, where the fluid at the surface flows radially outward (creating a circular talc-free region in the centre of the photograph) while a recirculating inward flow occurs near the bottom wall, as shown by the dye streak displacement towards the centre of the photograph. In contrast, figure 3(*b*) ($H_0 = 1$ mm) shows that the flow is unidirectionally outward throughout the film since both talc and dye streaks are carried away from the drop centre. Figure 3(*c*) demonstrates that the net outflow in thinner films ($H_0 = 0.4$ mm) leads to film thinning and eventually to film rupture at a finite, non-zero radius, indicated in the photograph by the white band. As shown by figure 3(*c*), glycerol covered with oleic acid remains in the central region (where the droplet was initially placed), and the talc-free region of the film surface extends past the rupture site. This profile did not change in time (>1 hour), suggesting that it was a stable configuration. Note that qualitatively similar rupture has been described by Fraaije & Cazabat (1989).

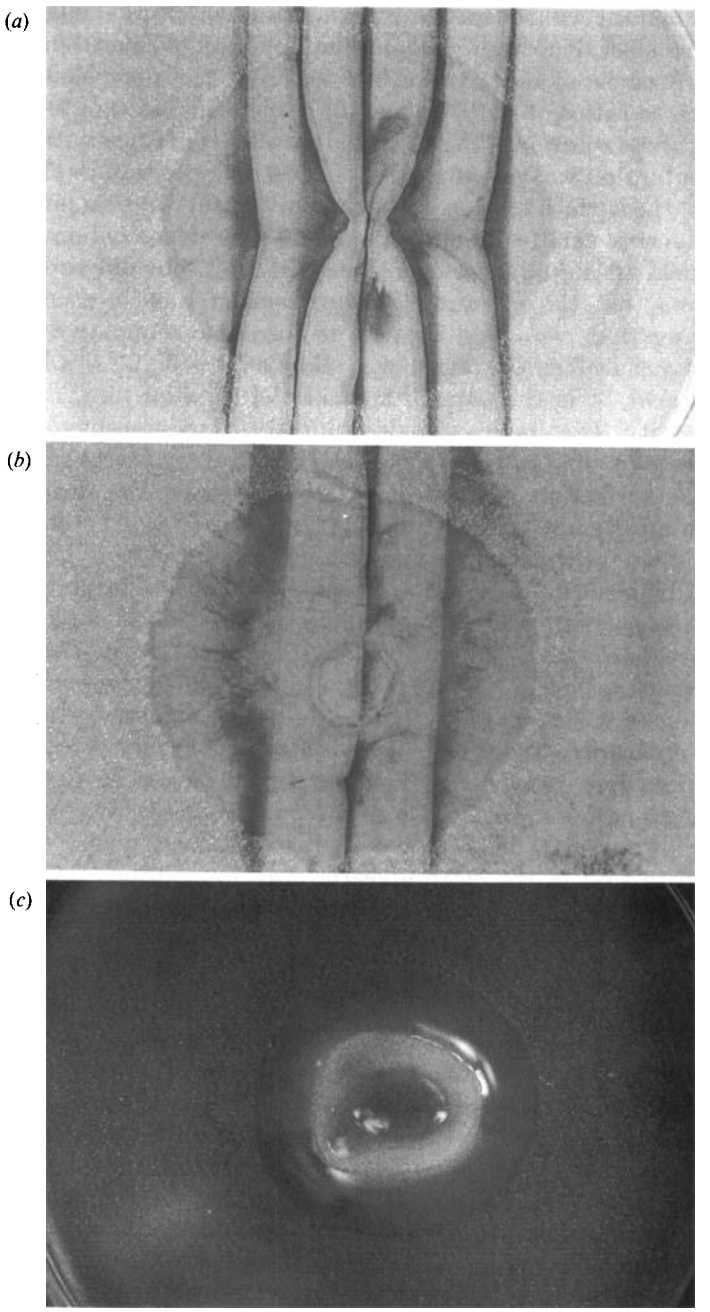

FIGURE 3(*a*). Photograph of flow visualization experiment, $H_0 = 2$ mm. The surface is initially dusted with talc. The circular region in the centre of the photograph represents the talc-free region, demonstrating outflow on the film surface. Inward deformation of the initially straight dye streaks indicates inward flow near bottom wall. This pattern illustrates bidirectional film flow. (*b*) Photograph of flow visualization experiment. $H_0 = 1$ mm. The surface is initially dusted with talc. The circular region in the centre of the photograph represents the talc-free region, demonstrating outflow on the film surface. Outward deformation of the initially straight dye streaks indicates outward flow near bottom wall. This pattern illustrates net outflow throughout the film. (*c*) Photograph of the flow visualization experiment, $H_0 = 0.4$ mm. The surface is initially dusted with talc. The white band denotes the location of the ruptured film. The large circular region indicates the talc-free region. Extension of talc-free region past the rupture site demonstrates that surfactant has spread past the rupture site.

3.2. *Quantitative measurements*

Since the laboratory temperature varied from day to day (but was constant during each individual experimental trial) the kinematic viscosity of the glycerol varied between experiments from 3.0 cm^2/s to 6.0 cm^2/s, as measured before and after each experiment with a bulb viscometer (Cannon–Fenske–Ostwald type 400 J788). To account for the variability of viscosity, the data (onset time for non-zero surface convection at a specified radial position) was represented non-dimensionally using the scales of Gaver & Grotberg (1990). This scaling is $r^* = R_0 r$, and $t^* = \mu R_0^2/(SH_0)t$, where μ is the film viscosity, and S is the 'spreading parameter' defined as $S = (\sigma_0 - \sigma_m)$. Figures 4(*a*) and 4(*b*) show the measured location of this time-dependent 'convection front' for experiments A and B respectively. Here, the experimental results are represented as a mean value for all experiments ($n_A = 10$, $n_B = 12$) with error bars representing the standard deviation of the mean. Surface velocities were smaller in experiment B than in experiment A, making the subjective determination of flow onset more difficult, and resulting in larger error bars.

4. Discussion

4.1. *Theoretical framework*

In Gaver & Grotberg (1990), the physical system is modelled as a thin film of Newtonian fluid with kinematic viscosity ν, and constant density ρ resting on a rigid surface, with the surfactant deposited on the film's air–liquid interface. The problem is posed in cylindrical coordinates, where the radial coordinate, r, lies along the rigid wall with its origin at the centre of the surfactant droplet; the axial coordinate, z, has its origin on the rigid surface, and circular symmetry is assumed. The position of the thin-film surface is defined by $z = H(r, t)$, and the concentration of surfactant is denoted by $\Gamma(r, t)$. The velocity vector, $\boldsymbol{v} = (v_r, 0, v_z)$, and evolution equations for film thickness, H, and surfactant concentration, Γ, are derived with the following governing equations: (i) the Navier–Stokes equations; (ii) conservation of mass of the film layer; (iii) conservation of insoluble surfactant at the interface, where the surfactant was allowed to diffuse along the surface with constant diffusivity D_s or convect along the surface of the thin film; (iv) the tangential-stress jump condition, representing the balance of the viscous stress at the film's interface with the surface-tension gradients created by the surfactant; (v) the surface-tension equation of state, representing the relationship between the concentration of surfactant and the interfacial surface tension; (vi) the normal-stress jump condition, introducing capillary forces due to surface curvature; (vii) the kinematic boundary condition, which specifies that fluid particles positioned at the free surface remain attached to that surface, and (viii) no-slip and no-penetration boundary conditions at the wall.

The governing equations were non-dimensionalized using the following dimensionless variables whose relation to the dimensional variables (denoted by *) are given by:

$$r^* = R_0 r, \quad z^* = H_0 z, \quad \sigma^* = \sigma_m + S\sigma, \quad v_r^* = Uv_r = \frac{SH_0}{\mu R_0} v_r,$$

$$v_z^* = \frac{H_0 U}{R_0} v_z, \quad t^* = Tt = \frac{\mu R_0^2}{SH_0} t, \quad \Gamma^* = \Gamma_m \Gamma, \quad P^* = \frac{S}{H_0} P,$$

the velocity scale, $U = SH_0/(\mu R_0)$, was found by scaling the tangential-stress condition for a flat interface, and the timescale, $T = R_0/U = \mu R_0^2/(S H_0)$, is

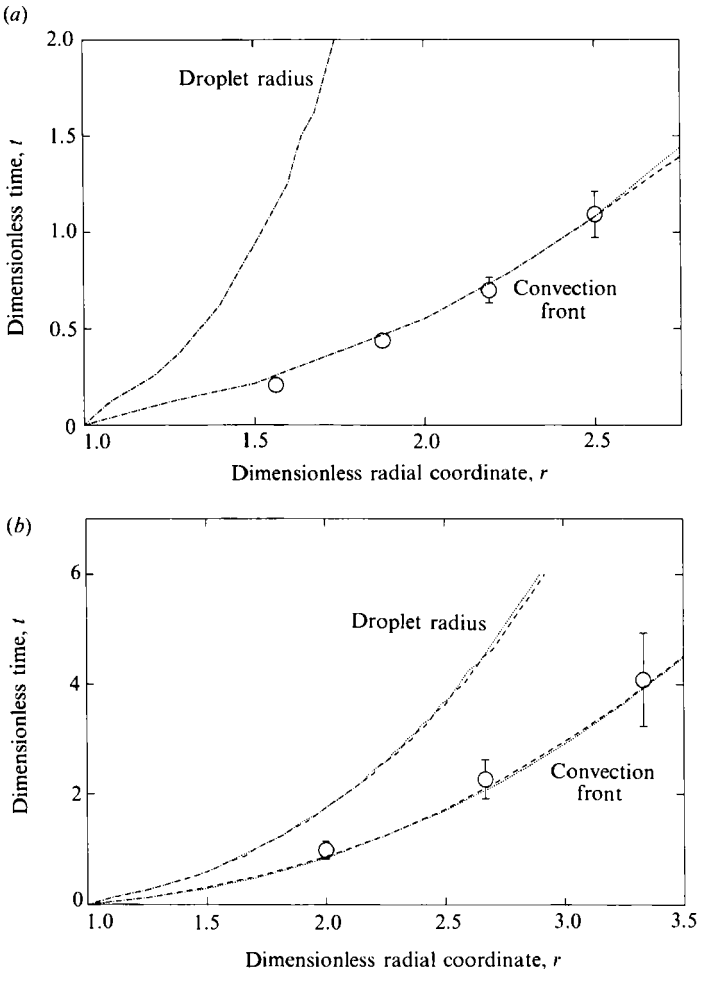

FIGURE 4(*a*). Experimentally and theoretically determined positions of the convection front and droplet leading edge for experiment A. $G = 2.0$; $\beta = 1.63$; $\Gamma_{max} = 1.36$; $\cdots$, $Pe_s = 2.1 \times 10^4$; ——, $Pe_s = 4.3 \times 10^5$. (*b*) Experimentally and theoretically determined positions of the convection front and droplet leading edge for experiment A. $G = 0.25$; $\beta = 1.63$; $\Gamma_{max} = 3.10$; $\cdots$, $Pe_s = 7.8 \times 10^4$, ——, $Pe_s = 9.8 \times 10^5$.

appropriate for convective events. Substituting this scaling into the governing equations produces the following dimensionless parameters:

$$\epsilon = \frac{H_0}{R_0}, \quad Re = \frac{UR_0}{\nu}, \quad G = \frac{\rho H_0^2 g}{S}, \quad Pe_s = \frac{UR_0}{D_s}, \quad \beta = \frac{\sigma_m}{S} = \frac{\sigma_0}{S} - 1.$$

Here ϵ is defined as the ratio of the vertical and radial lengthscales; Re is the Reynolds number, characterizing the relative magnitudes of the inertial and viscous forces in the fluid; G is the gravitational parameter, describing the ratio of the gravitational driving force to the surface-tension gradient (Marangoni) forcing; Pe_s is the surface Péclet number, which relates the transport of surfactant due to convection with that due to surface diffusion, and $\epsilon^2\beta$ represents the ratio of capillary driving forces to the driving forces due to surface-tension gradients. By taking the limit of $\epsilon \to 0$ (droplet diameter $\gg$ film thickness) lubrication analysis is employed. In

this limit, terms of $O(\epsilon^2 Re)$ and $O(\epsilon^2\beta)$ are vanishingly small, hence inertial and capillary forces may be neglected. From this analysis, the velocity field is found to be:

$$v_r(r,z,t) = G\frac{\partial H}{\partial r}\{\tfrac{1}{2}z^2 - zH\} + \frac{\partial\sigma}{\partial\Gamma}\frac{\partial\Gamma}{\partial r}z, \tag{4.1a}$$

$$v_z(r,z,t) = \frac{1}{r}\frac{\partial}{\partial r}\left\{r\left[G\frac{\partial H}{\partial r}(\tfrac{1}{2}z^2 H - \tfrac{1}{6}z^3) - \tfrac{1}{2}z^2\frac{\partial\sigma}{\partial\Gamma}\frac{\partial\Gamma}{\partial r}\right]\right\}. \tag{4.1b}$$

Equations (4.1 *a*, *b*) were used to calculate the evolution equations for H and Γ, which are:

$$\frac{\partial H}{\partial t} = \frac{1}{r}\frac{\partial}{\partial r}\left\{r\left[\tfrac{1}{3}G\frac{\partial H}{\partial r}H^3 - \tfrac{1}{2}H^2\frac{\partial\sigma}{\partial\Gamma}\frac{\partial\Gamma}{\partial r}\right]\right\}, \tag{4.2}$$

$$\frac{\partial\Gamma}{\partial t} = \frac{1}{r}\frac{\partial}{\partial r}\left\{r\left[\left(\frac{1}{Pe_s} - \Gamma H\frac{\partial\sigma}{\partial\Gamma}\right)\frac{\partial\Gamma}{\partial r} + \tfrac{1}{2}G\Gamma H^2\frac{\partial H}{\partial r}\right]\right\}. \tag{4.3}$$

The solutions to (4.2) and (4.3) were computed numerically by the 'Method of Lines', with the initial conditions:

$$\left.\begin{aligned} \Gamma(r,0) &= \begin{cases} \Gamma_{\max} & r \leqslant RI, \\ \Gamma_{\max}\left\{0.5\cos\left[\dfrac{\pi(r-RI)}{1-RI}\right]+0.5\right\} & RI < r \leqslant 1.0, \\ 0 & r > 1.0, \end{cases} \\ H(r,0) &= 1 \qquad\qquad r \geqslant 0, \end{aligned}\right\} \tag{4.4}$$

where RI is an adjustable parameter that defines the location of the initial non-zero surface-concentration gradients as $RI < r < 1$.

Predictions from this theory rely upon a surface-tension equation of state that relates the surface tension (σ^*) to the surfactant concentration (Γ^*). We use a modified form of the equation of state derived by Sheludko (1967) that is suitable for $\Gamma^* > \Gamma_m$,

$$\left.\begin{aligned} &\Gamma^* < 0.8\Gamma_m\colon \quad \sigma^* = \sigma^*(\Gamma^*) = \frac{\sigma_0}{(1+\theta\Gamma^*/\Gamma_m)^3} = f(\Gamma^*), \\ &\Gamma^* \geqslant 0.8\Gamma_m\colon \quad \sigma^* = A\exp[-B(\Gamma^*/\Gamma_m - 0.8)] + \sigma_m, \\ &\text{where} \qquad \theta = (\sigma_0/\sigma_m)^{\frac{1}{3}} - 1, A = f(0.8\Gamma_m) - \sigma_m, \quad B = \frac{3\sigma_0\theta}{A(1+0.8\theta)^4}. \end{aligned}\right\} \tag{4.5}$$

As demonstrated by figure 2(*b*), this equation of state is a faithful representation of the experimentally determined relationship between the surface tension and surfactant concentration.

To compare the results of this analysis with the experimental observations of the convection patterns, the Lagrangian motion of individual fluid 'particles' within the film was calculated. In addition, the time-dependent trajectories of surface particles were computed for comparison with the measurements of surface dye-marker motion. To find these trajectories, the Lagrangian equations of motion,

$$\frac{\mathrm{d}\boldsymbol{X}}{\mathrm{d}t} = \boldsymbol{v}(\boldsymbol{X},t) \tag{4.6}$$

were integrated. Here, $\boldsymbol{v}(\boldsymbol{X},t)$ is the Eulerian velocity field (equations (4.1 *a*, *b*)) at

H_0 (mm)	G	β	Pe_s
2	≈ 2.0	1.63	$\approx 10^4$
1	≈ 0.5	1.63	$\approx 10^4$

TABLE 2. Dimensionless parameter estimates of the flow visualization experiments

$\boldsymbol{x} = \boldsymbol{X}$ at time t, and $\boldsymbol{X} = \boldsymbol{X}(\boldsymbol{X}_0, t)$ is the position of the particle whose initial position is $\boldsymbol{X}_0$ at time t_0. Equation (4.6) was numerically integrated using a fourth-order Runge–Kutta method, where the timestep was adjusted so that particles initially on the air–liquid interface remained on that material surface.

4.2. *Comparison of qualitative flow pattern observations with theoretical predictions*

To investigate the parametric dependency of the particle trajectories, the Lagrangian motion of a set of fluid particles within the thin film was calculated. Since the flow-visualization experiments did not begin with a well-defined droplet radius, the magnitude of the dimensionless parameter $\epsilon = H_0/R_0$ remains undetermined but is assumed to be small, since the initial film thickness is very small. G, Pe_s and β are dependent of R_0, and their approximate magnitudes are listed in table 2.

Figures 5(*a*) and 5(*b*) show the predicted particle path trajectories for experiments commencing with initial conditions specified in table 2 and $\Gamma_{\max} = 10.0$. It should be noted that these simulations were computed over different durations of dimensionless time, with $\Delta t_{H_0=2\,\mathrm{mm}} = 100$, and $\Delta t_{H_0=1\,\mathrm{mm}} = 50$. These choices, however, correspond to equivalent durations of dimensional time, approximately 30 s after $R_0 = 0.5$ cm. Also, these simulations are based upon maximum surfactant concentrations that are much smaller than those used in the actual experiments (where a drop of pure oleic acid was placed directly on the film). This discrepancy between the initial conditions used in the simulations and experiments was necessitated by the fact that larger concentrations led to marked film thinning that became numerically unstable and disrupted the numerical calculations. Nevertheless, the simulations show good agreement with the qualitative flow behaviour. Similar to the experimental observations of flows in a 2 mm film (figure 3*a*), figure 5(*a*) shows that flow reversal causes the particles near the bottom wall to have a net inward displacement, and particles near the film surface have a net outward displacement (bidirectional flow). In contrast, figures 3(*b*) and 5(*b*) demonstrate that the flows within thinner films (1 mm) are uniformly outward, and flow reversal does not bring the particles near the wall radially inward of their initial positions. Figure 3(*c*) shows that the spreading of a surfactant on an exceedingly thin film causes the film to rupture at a finite radius. The final film profile shown in figure 5(*b*) shows marked thinning at $r \approx 2.5$, suggesting the possibility of film rupture in that vicinity when G is small. Should the film rupture at that location, surfactant would lie in both the central region and beyond the rupture, as was observed experimentally (figure 3*c*). We find it interesting that the computed particle trajectories show that particles initially beneath the droplet's leading edge convect to positions near the film surface, even though their initial positions may be near the bottom wall. Clearly, gravitationally-induced recirculation leads to the replacement of these particles by their neighbours (figure 5*a*), and stabilizes the film. This recirculation is shown in the streamline descriptions of Gaver & Grotberg (1990). If hydrostatic pressure gradients are small (small G), these particles are not replaced, and the film thins.

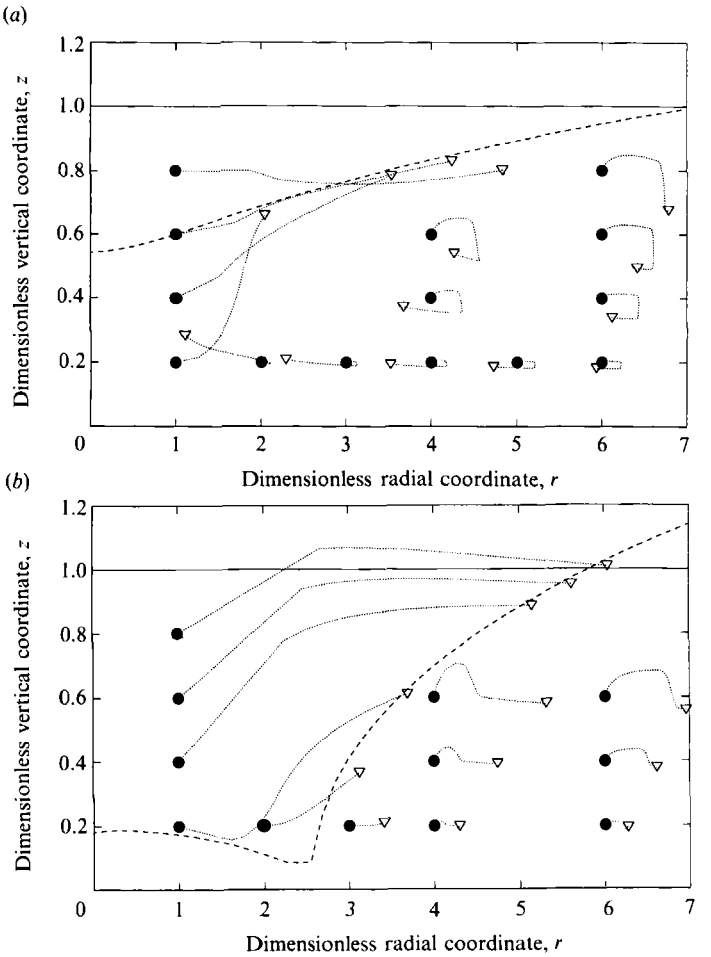

FIGURE 5(*a*). Calculated particle path trajectories corresponding to figure 3(*a*). $G = 2.0$; $\beta = 1.63$, $Pe_s = 10^4$; $\Gamma_{max} = 10.0$; $\Delta t = 100$; ——, initial film profile; – – –, final film profile; ●, initial particle positions; ▽, final particle positions; ..., particle trajectories. (*b*) Calculated particle path trajectories corresponding to figure 3(*b*). $G = 0.5$; $\beta = 1.63$, $Pe_s = 10^4$; $\Gamma_{max} = 10.0$; $\Delta t = 50$; ——, initial film profile; – – –, final film profile; ●, initial particle positions; ▽, final particle positions; ..., particle trajectories.

The study of the qualitative flow behaviour demonstrates the Lagrangian field's strong dependency on the gravitational parameter, $G = \rho g H_0^2/S$. When $G > 0$, the deposition of surfactant induces a build-up of fluid near the surfactant's leading edge. Eventually, gravitational forces counter this welling mechanism, and create a flow reversal within the film in the form of a ring vortex near the bottom wall, creating bidirectional flow. As G decreases, flow reversal is delayed owing to a commensurate decrease in the hydrostatic gradient. Flow-reversal onset times could not be computed for large Γ because of substantial numerical instability that occurred as H thinned ($H < 0.05$) prior to flow reversal. For this reason the flow-reversal onset times were computed for $\Gamma = 0.5$, 1.0 and 1.5 with $\beta = 1.63$, $RI = 0.7$, and $Pe_s = 10^4$. The results of this computation (figure 6) show that when $G > 1$, flow reversal occurs almost instantly after surfactant deposition, so outflow at the surface is quickly accompanied by inflow near the bottom wall. This behaviour is described by figures 3(*a*) and 5(*a*), where bi-directional flow is clearly evident. As G decreases to values

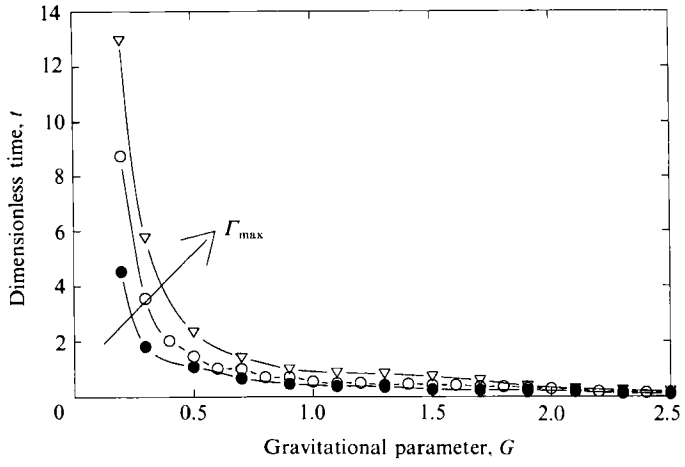

FIGURE 6. Flow reversal onset time *vs.* G for $Pe_s = 10^4$; $\beta = 1.63$; $RI = 0.7$; ●, $\Gamma_{max} = 0.5$; ○, 1.0; ▽, 1.5.

smaller than 0.5, however, the flow-reversal onset time increases dramatically, leading to prolonged outflow. This behaviour is demonstrated by figures 3(*b*) and 5(*b*) where outflow occurs for the duration of the experiment. Figure 6 also demonstrates that flow reversal onset times are qualitatively independent of Γ_{max}, which suggests that simulations based upon $\Gamma_{max} = 1$ may be roughly compared with experiments where $\Gamma_{max} > 1$.

4.3. *Comparison of quantitative surface-flow measurements with theoretical predictions*

To compare the quantitative experimental measurements with the simulation results, we devised an equivalent theoretical experiment from which to base the predictions. In the benchtop experiments, the onset time for surface dye-marker motion was measured by the small displacement of the marker from its initial position. Correspondingly, the predictions were based upon the time it took a surface fluid particle to advect a small distance. This motion reflects the onset of large-scale surface convection at the radius marked by that particle, and thus defines the position of the convection front. To predict the position of the convection front, a set of surface fluid particles was tracked as the surfactant spread. A criterion was set for the onset of particle motion that was equivalent, in dimensional terms, to having the particle move 0.075 cm. This criterion is *ad hoc*, but seems reasonable since it reflects the resolution of the experiments. In addition, the droplet radius is of interest. Since we were incapable of measuring the position of the droplet's leading edge during the experiments, its location was predicted using our theory, and will be shown in relation to the position of the convection front. For this purpose, the droplet radius, r_D, is defined by

$$0.95\, V_{surf} = 2\pi \int_0^{r_D} r\Gamma(r,t)\, dr, \tag{4.7}$$

a definition that is identical to that used in Gaver & Grotberg (1990).

Table 3 summarizes the magnitudes of the dimensionless parameters representative of experiments A and B, and shows that in these experiments, $\epsilon \ll 1$, $\epsilon^2 Re \ll 1$, and $\epsilon^2 \beta \ll 1$, so neglecting terms of their magnitude in the theory is

Expt	G	β	$(Pe_s)_{max}$ (10^5)	$(Pe_s)_{min}$ (10^4)	Γ_{max}	ϵ	$\epsilon^2\beta$ (10^{-2})	$\epsilon^2 Re$ (10^{-4})
A	2.0	1.63	4.3	2.1	1.36	0.12	2.3	2.5
B	0.25	1.63	9.8	7.8	3.10	0.09	1.3	1.4

TABLE 3. Dimensionless parameter magnitudes of Experiments A and B

justified when making predictions of this system. Here the surface Péclet number, Pe_s, is based upon surface diffusivities in the range

$$1 \times 10^{-6}\ \text{cm}^2/\text{s} < D_s < 1 \times 10^{-4}\ \text{cm}^2/\text{s},$$

(Flood, 1967; Good & Schechter 1972; Agrawal & Neuman 1988). The large values of Pe_s indicate that most of the transport of the surfactant was due to convection, and not surface diffusion. The theory shows that in the limiting case of $Pe_s \to \infty$ the surfactant spreads as a moving 'shock', and creates a convection front as described above. Below, it will be shown that the velocity is independent of the relatively small change in Pe_s between $(Pe_s)_{min}$ and $(Pe_s)_{max}$. For this reason, the experimental data, when put in dimensionless form, is adequately represented by two plots – one for data taken from experiments commencing with initial condition set A, and one for data taken from experiments beginning with initial condition set B.

Whereas the experimental protocol creates initially steep concentration gradients near $r = 1$, predictions were made by specifying $RI = 0.7$, thus locating the initial concentration gradients between $0.7 < r < 1$ (maximum gradient at $r = 0.85$), the largest value of RI that provides numerically stable results. However, it was shown in Gaver & Grotberg (1990) that the film profiles near the leading edge are a robust function of RI or a given volume of surfactant (V_{surf}). Since this film thickness perturbation provides the gravitational forcing that determines the position of the convection front relative to the droplet leading edge, the calculations should provide results that are comparable to experiments in which $RI = 1$. Assuming $RI = 0.7$, and a surfactant distribution provided by (4.4),

$$\Gamma_{max} = \frac{V_{surf}}{0.73\pi R_0^2 \Gamma_m}. \tag{4.8}$$

The values of G and β in table 3 were used to predict the position of the convection front and droplet radius for experiments commencing with initial condition sets A and B. Since Pe_s remains unspecified, calculations were performed for Pe_s equal to $(Pe_s)_{min}$ and $(Pe_s)_{max}$. These predictions create an extremely small envelope, shown in figures 4(*a*) and 4(*b*), which demonstrate the insensitivity of the spreading rate to Pe_s when Pe_s is large. This insensitivity permits the representation of the experimental data on only two graphs. These figures show that the predicted position of the convection front, r_{CF}, is in strong agreement with the experimental measurements. Figure 4 also shows the predicted position of the droplet radius, r_D. Apparently, gravitationally induced flows extend beyond the droplet's leading edge because of welling of the fluid induced by the Marangoni forcing, causing $r_{CF} > r_D$.

The calculated values of the droplet radius, r_D, and convection front radius, r_{CF}, were regressed to the form $r_D - 1 = K_1 t^{K_2}$. The results of this regression are:

Experiment A:

$$r_D - 1 = 0.74 t^{0.73} \quad (R^2 = 0.96),$$
$$r_{CF} - 1 = 1.14 t^{0.70} \quad (R^2 = 0.96),$$

Experiment B:

$$r_D - 1 = 0.85 t^{0.80} \quad (R^2 = 0.98),$$

$$r_{CF} - 1 = 1.01 t^{0.63} \quad (R^2 = 0.98).$$

While these regressions do not represent closed-form solutions of the spreading droplet problem, they simply and accurately represent the location of the time-dependent positions of the droplet's leading edge and convection front. Unfortunately, the dependence of K_1 and K_2 upon the dimensionless parameters G, Pe_s and β remains unresolved. Nevertheless, these regressions should help facilitate comparison of our results with those of other investigators.

As demonstrated by figure 4, the experimentally determined position of the convection front is in very close agreement with position predicted by the theory of Gaver & Grotberg (1990). Deviations may be attributed to differences between the experimental protocol and the theoretical assumptions. First, by lifting the restraining collar to initiate the experiment, gravity and capillarity waves are produced which may propagate through the film and obscure the motion induced by Marangoni convection. To investigate this phenomena, we observed the motion of the dye markers after the withdrawal of the restraining collar without surfactant. This removal caused only slight motion (less than 2 mm total deflection) of the first flow visualization marker, which quickly returned to its initial position. Such motion was due to the collar first pulling, then releasing the fluid from the film as the collar was removed, and thus is due to conservation of mass. Following Lighthill (1978), any capillary/gravity waves of length $\lambda \leqslant R_0$ attenuate to $1/e$ of their initial energy in a distance less than 10^{-3} cm from the collar for both experiments A and B. This system thus overdamps capillary/gravity waves, preventing them from influencing the surfactant spreading.

Another discrepancy between theory and experiment occurs in the assumption of the initial surfactant distribution. As described above, the experiments commence with a sharp decrease in surfactant concentration at $r^* = R_0$. This condition cannot be replicated in the theoretical evaluation since the numerical solution becomes unstable if the location of the initial concentration gradient is centred beyond $r^* > 0.85\ R_0$ ($RI = 0.7$). Fortunately, the initial concentration gradients rapidly redistribute by Marangoni convection, and thus much of the longterm spreading behaviour is dominated by the volume of surfactant (V_{surf}) and not the location of the initial concentration gradient (Gaver & Grotberg 1990). Consequently, this source of error is not expected to be appreciable. Further errors may be attributed to lack of automation of the collar removal, which may be responsible for the variation of the measured convection-front velocity. Finally, additional errors may be induced by a fingering instability which was reported by Troian, Wu & Safran (1989) to exist at the outer edge of surfactant spreading on thin films. This instability is hypothesized by Troian, Herbolzheimer & Safran (1990) to be due to adverse mobility gradients near the droplet leading edge. We did not attempt to observe this instability, but such a phenomena would lead to variability in the location of the droplet leading edge, and hence to inconsistency in the location of the convection front. Such behaviour may be partially responsible for the experimental errors shown in figure 4.

5. Conclusions

We have investigated the spread of oleic acid on thin glycerol films experimentally. The resulting flow field is described both qualitatively and quantitatively, and

demonstrates a range of behaviours that depend upon the initial film thickness, H_0. It was found that changing H_0 leads primarily to modification of the relative gravitational forcing (tables 2 and 3), represented by the parameter $G = \rho H_0^2 g/S$. For small G, the film is subject to net outflow for all t, leading to film thinning and the possibility of rupture. In contrast, larger G causes bidirectional flow that is induced by hydrostatic pressure gradients. This flow behaviour agrees with our predictions, as can be seen from the comparison of Figures 3(a, b) and 5(a, b). Additionally, surface-flow measurements correlate extremely well with the theoretical predictions (figure 4).

The favourable comparison of the observed flow behaviour and measured surface velocities appears to validate our theory. A well-defined convection front appears to exist, which allows measurement of the surface flows. Such a front is predicted by Borgas & Grotberg (1988) and Gaver & Grotberg (1990), where in the limit of $1/Pe_s \to 0$ and $G \to 0$, a step discontinuity occurs in film height at the droplet leading edge, and a commensurate velocity jump develops in that vicinity. While film disturbances were observable owing to the diffraction of light through the curved interface, we did not observe a sharp jump in film height, presumably because gravity and capillarity modify the shock structure. Nevertheless, the strong correlation between the theoretical predictions and experimental measurements suggest that the fine characteristics of the leading edge play only a minor role in determining the overall spreading behaviour.

A number of heretofore unrecognized flow and film characteristics arising from the deposition of surfactant on the thin film are also described here. These include the distinction between the convection front and droplet leading edge. As detailed above, the convection front is not coincident with the droplet leading edge because of gravitationally-induced flows caused by the welling of fluid near the droplet's leading edge. As demonstrated by figure 4, these differences may be substantial even in experiments where $G \ll 1$. Since most measurements of surface flows are conducted with surface markers (e.g. talc), it is important to recognize that these measurements reflect the position of the convection front, and not the position of the droplet's leading edge.

The small-G experiments demonstrated film rupture induced by the localized surfactant. This behaviour is caused by the net outflow of the film in the region of the largest surface-tension gradients near the droplet leading edge. Predictions from the theory show film profiles strikingly similar to these observations (compare figures 3c and 5b), suggesting that most of the ruptured-film characteristics are determined by the dynamics of the surfactant-induced flows and not the mechanics of the rupturing interface. Ahmad & Hansen (1972) also found film rupture in their planar experiments, apparently for all film thicknesses tested. This may be due to their large initial surfactant concentrations. Additionally, Fraaije & Cazabat (1989) reported similar film rupture behaviour.

How do the results of this study relate to surfactant and medication delivery by aerosol inhalation? Under normal circumstances, the lung's liquid lining is thin enough to make gravitational effects small, although some disease states may make its thickness and gravity effects appreciable. For small gravity effects, this study cautions that film rupture may occur, especially if the surface Péclet number ($Pe_s = SH_0/\mu D_s$) is large. However, Gaver & Grotberg (1990) show that the risk of film rupture diminishes as Pe_s decreases. Analysis of medication delivery through the lung's liquid lining depends upon an understanding of the convection–diffusion process through the film. In this problem the leading-order flow field is caused by the

spreading droplet. As these studies show, the spreading surfactant not only induces flows within the film, but also modifies the film thickness, through which the medication must be transported. Depending upon the magnitude of the film Péclet number, the surfactant-induced flows may influence the rate and pattern of medication delivery to the airway wall and hence the delivery of medication.

Technical assistance was provided by Mr W. Liebkemann, whose help is appreciated. D.P.G. is a Parker B. Francis Fellow in Pulmonary Research. This research was funded by a grant from the Whitaker Foundation, and NIH grants K04-HL01818 and R01-HL41126.

REFERENCES

AGRAWAL, M. L. & NEUMAN, R. D. 1988 Surface diffusion in monomolecular films, II. experiment and theory. *J. Colloid Interface Sci.* **121**(2), 366–379.

AHMAD, J. & HANSEN, R. S. 1972 A simple quantitative treatment of the spreading of monolayers on thin liquid films. *J. Colloid Interface Sci.* **38**, 601–604.

AVERY, M. E. & MERRITT, T. A. 1991 Surfactant replacement therapy. *N. Engl. J. Med.* **324**(13), 910–911.

BORGAS, M. S. & GROTBERG, J. B. 1988 Monolayer flow on a thin film. *J. Fluid Mech.* **193**, 151–170.

CONTE, J. E., HOLLANDER, H. & GOLDEN, J. A. 1987 Inhaled or reduced-dose intravenous pentamidine for *Pneumocystis carinii* pneumonia. *Ann. Int. Med.* **107**, 495–498.

FLOOD, E. A. 1967 *The Solid-Gas Interface*, pp. 582–586. Marcel Dekker.

FRAAIJE, J. G. E. M. & CAZABAT, A. M. 1989 Dynamics of spreading on a liquid substrate. *J. Colloid Interface Sci.* **133**(2), 452–460.

GAINES, G. L. 1966 *Insoluble Monolayers at Gas Liquid Interfaces*. Wiley Interscience.

GAVER, D. P., III, & GROTBERG, J. B. 1990 The dynamics of a localized surfactant on a thin film. *J. Fluid Mech.* **213**, 127–148.

GAVER, D. P., III, SAMSEL, R. W. & SOLWAY, J. 1990 The effect of surface tension and viscosity on airway reopening. *J. Appl. Physiol.* **69**(1), 74–85.

GOOD, P. A. & SCHECHTER, R. S. 1972 Surface diffusion in monolayers. *J. Colloid Interface Sci.* **40**(1), 99–106.

HALPERN, D. & GROTBERG, J. B. 1990 Interfacial dynamics in the pulmonary system. Society for Industrial and Applied Mathematics Annual Meeting, Chicago, Illinois, July, 1990.

HUSSAIN, Z., FATIMA, M. & AHMAD, J. 1975 The rate of spreading of monolayers on liquids. *J. Colloid Interface Sci.* **50**, 44–48.

LIGHTHILL, J. 1978 *Waves in Fluids*. Cambridge University Press.

RUCKENSTEIN, E., SMIGELSCHI, O. & SUCIU, D. G. 1970 A steady dissolving drop method for studying the pure Marangoni effect. *Chem. Engng. Sci.* **25**, 1249–1254.

SHELUDKO, A. 1967 *Adv. Colloid Interface Sci.* **1**, 391–464.

TROIAN, S. M., HERBOLZHEIMER, E. & SAFRAN, S. A. 1990 Model for the fingering instability of spreading surfactant drops. *Phys. Rev. Lett.* **65**(3), 333–336.

TROIAN, S. M., WU, X. L. & SAFRAN, S. A. 1989 Fingering instability in thin wetting films. *Phys. Rev. Lett.* **62**(13), 1496–1499.